Single-photon time-of-flight measurements for benchmarking time transfer in quantum networks

DONGXING HE[1,2], PAULINA S. KUO[1,*], YA-SHIAN LI-BABOUD[1], ANOUAR RAHMOUNI[1], MATTHEW D. SHAW[3], BORIS A. KORZH[3,4], AND THOMAS GERRITS[1]

[1] National Institute of Standards and Technology, Gaithersburg, Maryland 20899, USA
[2] University of Maryland, College Park, Maryland 20742, USA
[3] Jet Propulsion Laboratory, California Institute of Technology, Pasadena, California 91125, USA
[4] Group of Applied Physics, University of Geneva, 1205 Geneva, Switzerland
[*] paulina.kuo@nist.gov

Compiled November 18, 2025

We propose a single-photon time-of-flight (ToF) measurement method to benchmark fiber-path delay estimation in optical two-way time and frequency transfer (OTWTFT) protocols. The single-photon ToF measurement yields uncertainties better than 2 ps (0.5 mm fiber-path length uncertainty) at 1 s integration times for a deployed 120 km (loopback) fiber. Differences between the ToF and the roundtrip time measurements from a White Rabbit Precision Time Protocol appear to correlate with the clock phase error between two White Rabbit switches. The results suggest that augmenting single-photon ToF measurements with existing OTWTFT protocols could enhance the precision to sub-10 ps levels at metropolitan distances. Such level of precision will be critical for synchronization in quantum networks.

http://dx.doi.org/10.1364/ao.XX.XXXXXX

1. INTRODUCTION

Integration of standards-based optical two-way time-frequency transfer (OTWTFT) methods can serve as a readily deployable solution for quantum networks. Co-propagation of quantum and classical time synchronization signals [1, 2] along with entanglement swapping capabilities will be essential to scaling the number of nodes, range, and rates of quantum-network protocols. Entanglement swapping will require photons to arrive at a detection plane within a bounded coherence time. High-precision time synchronization on the order of < 10 ps will be beneficial in advancing the rates and ranges for many protocols requiring entanglement distribution and swapping that rely on high-precision time stamping.

The White Rabbit Precision Time Protocol (WR-PTP) [3] has been demonstrated to provide < 10 ps time stability in a laboratory [4], and < 200 ps maximum time-interval error over aerial fiber at metropolitan-scale distances [5]. WR-PTP is capable of supporting the co-propagation of quantum and classical signals, with Bell-certified polarization entanglement distribution [2]. The protocol is part of the High-Accuracy Precision Time Protocol Profile [6] and is based on the Ethernet and Synchronous Ethernet [7, 8] standards to support low-cost scalability and enabling the time-transfer signal to be multiplexed with other classical and quantum channels.

OTWTFT methods rely on accurate measurements of the one-way path delay between the transmitted timestamp and the received timestamp at the remote clock. To achieve the sub-nanosecond clock-synchronization, calibrated roundtrip times (CRTT), are measured by the remote WR-PTP node at each synchronization interval using the digital dual mixer time difference (DDMTD) measurement method [9–11]. DDMTD allows sub-picosecond phase detection [12]. The fiber asymmetry can be caused by differences in the transmitter-to-receiver and receiver-to-transmitter paths used or by different group delays when two separate wavelengths are used for transmitting and receiving the timing signal over a single strand of fiber. The fiber asymmetry coefficient, α, is given by [3, 13]

$$\alpha = \frac{\Delta t_{\mathrm{TtoR}} - \Delta t_{\mathrm{RtoT}}}{\Delta t_{\mathrm{RtoT}}}, \tag{1}$$

where Δt_{TtoR} is the one-way path delay from the transmitter to the receiver, and Δt_{RtoT} is the delay from receiver to transmitter.

WR-PTP estimates the one-way delay between the transmitter and the receiver from the roundtrip time measurement [3], Δt_{WR}, and the sum of fixed delays at the transmitter and receiver, $\sum \Delta$. The one-way fiber path delay, Δt_{TtoR}, can be derived from the roundtrip time measurement by [3]:

$$\Delta t_{\mathrm{TtoR}} = \frac{1+\alpha}{2+\alpha}(\Delta t_{\mathrm{WR}} - \sum \Delta) \tag{2}$$

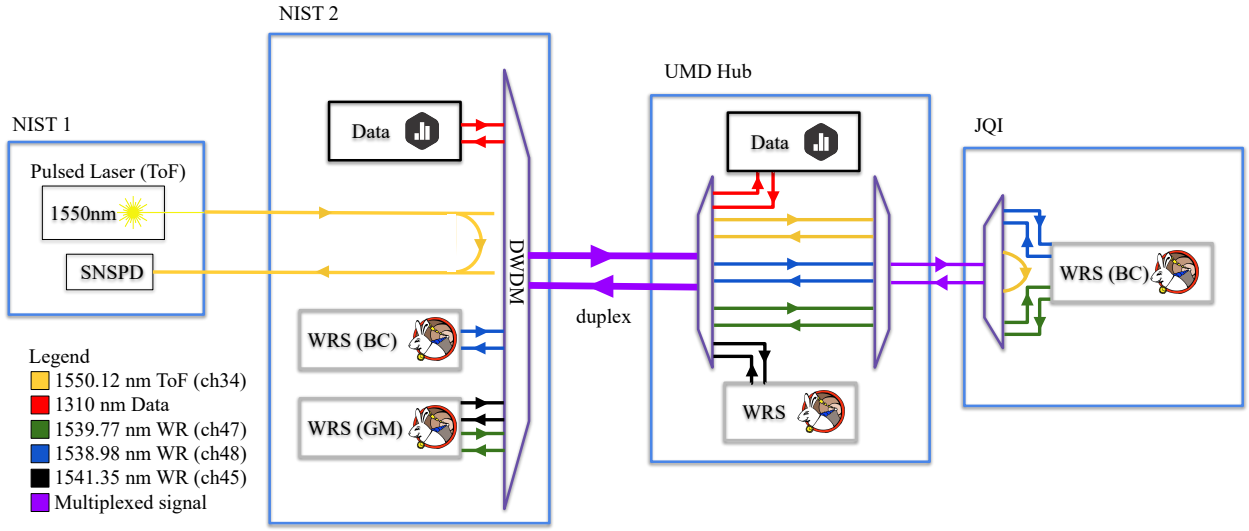

Fig. 1. The experimental setup included a 1550 nm pulsed laser with a co-located SNSPD in the same laboratory for the ≈120 km loopback time-of-flight measurements at single photon levels. The WRS GM and a WRS BC were also co-located at a separate NIST laboratory to obtain the phase error between both clocks and fiber-roundtrip-time measurements. The WRS GM supported three ITU-T DWDM channels 45, 47, and 48. The WRS BC at JQI received channel 47 from the GM and transmitted channel 48 to the WRS BC at NIST. Channel 45 was used to synchronize the WRS-BC at the UMD Hub.

Timestamps at the reference, t_1, and remote, t_2, clocks, are used to correct the remote clock's servo. The time error between the clocks, $\varepsilon_{\text{clock}}$, is

$$\varepsilon_{\text{clock}} = t_2 - t_1 - \Delta t_{\text{TtoR}}. \tag{3}$$

Therefore, an accurate, in-situ calibration of one-way path delay is one capability to enable higher precision time synchronization. We propose to apply single-photon time-of-flight (ToF) measurements to benchmark the one-way fiber path delay measurement of classical OTWTT methods for quantum networking applications. The single-photon ToF measurements can provide high temporal, and therefore longitudinal spatial resolution while also minimizing noise in co-propagating quantum channels. In contrast, telecommunication transceivers utilize bright classical signals for path delay estimation, which can degrade quantum channels due to cross-talk and Raman scattering. The time resolution that can be achieved for the single-photon ToF is limited by the laser pulse width, the single-photon detector timing jitter, and, combined with the laser bandwidth, the chromatic dispersion of the fiber. Superconducting nanowire single photon detectors (SNSPDs) have demonstrated high efficiency and low timing jitter to provide the signal-to-noise ratio (SNR) needed for long-range measurements.

Here, we present an implementation of a single-photon ToF fiber length characterization at 1550 nm and compare the resulting ToF roundtrip time measurements, Δt_{ToF} with WR roundtrip time measurements, Δt_{WR}. Our measurement was carried out on a deployed, ≈120 km loopback between NIST and the Joint Quantum Institute (JQI) at the University of Maryland (UMD). The WR system was run with low-phase-drift calibration. We demonstrate higher stability of the single-photon ToF as compared to the WR measurement. These higher stability measurements could be integrated into a WR clock servo correction algorithm potentially improving the synchronization precision.

2. EXPERIMENT

A. Topology

Figure 1 shows a schematic of our topology for the WR and ToF roundtrip time measurement comparison. Two laboratories are utilized at NIST for the pulsed laser and SNSPDs experimental setup (NIST 1), and NIST 2 for the experimental setup with White Rabbit Switches (WRS). Using dense wavelength division multiplexing (DWDM), we combined four wavelengths for the WR-PTP (ch47, ch48, ch45) and classical communication traffic (1310 nm). The single-photon pulses reside at 1550.12 nm (ch34) in the same ≈60 km fiber strand to a hub at UMD. At the UMD hub, we demultiplex the data traffic and one WR signal (ch45). The ch45 signals are not relevant for this study, but were present during our measurements. At the UMD hub, two WR signals and the single-photon pulses are further muxed/demuxed to our WRS boundary clock (BC) at JQI. This topology allows us to compare the roundtrip time between NIST and JQI based on the WR and the single-photon ToF measurements.

Furthermore, having a second BC at NIST allows measuring the phase error between the grandmaster (GM) at NIST and the BC at NIST [4]. The phase error, $\varepsilon_{\text{clock}}$, between the GM and BC at NIST is the time-varying offset between the two clocks and can be measured by time-stamping and evaluating the difference between both 10 MHz clock signals (see Eq. 3). At JQI, the single-photon pulse is looped back through a fiber cross-connect at the DWDM. The fiber lengths of the ToF single-photon pulse are carefully matched in each location to the fiber lengths utilized by the WR system to get a more accurate measurement of the deployed fiber distance. Therefore, we use a fiber splitter to add a local fiber loop at NIST in lab NIST2 to produce the start peak, which represents the start of the JQI fiber loop and therefore the start of the ToF measurement. This will result in two time peaks to appear on the single-photon detection apparatus (from the short loop and the long JQI loop). The difference between the peaks is the measured roundtrip time between NIST 2 and JQI, which we call $\Delta t'_{\text{ToF}}$. We note that $\Delta t'_{\text{ToF}}$ is not the actual

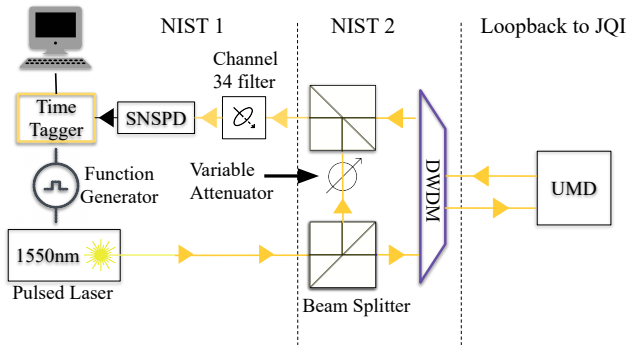

Fig. 2. A more detailed schematic of only the ToF measurement setup. NIST 1 and NIST 2 are located about 250 m apart on the NIST Gaithersburg campus. A function generator is used both as a trigger for the pulsed laser and for the Time Tagger.

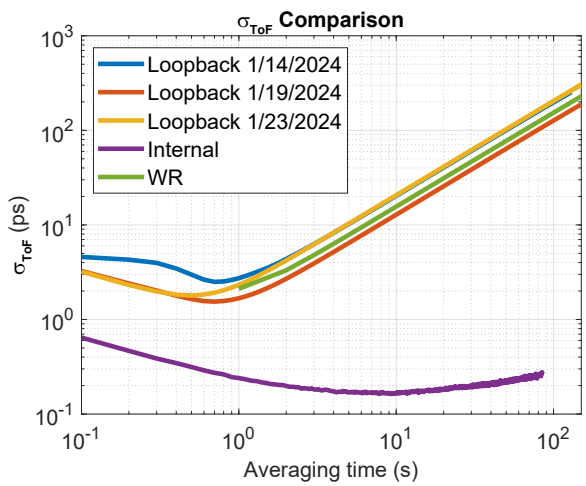

Fig. 3. σ_{ToF} comparisons between 1/14/2024, 1/19/2024, and 1/23/2024 ToF measurements as well as ToF measurement on only the NIST internal loopback, and the WR roundtrip data. Note that the WR roundtrip data starts at an averaging time of 1 second.

roundtrip time, which is on the order of 600 μs, but the relative location between both observed peaks. The actual roundtrip time, Δt_{ToF}, is

$$\Delta t_{\mathrm{ToF}} = \Delta t'_{\mathrm{ToF}} + N\tau_{\text{probe laser}}, \tag{4}$$

where N is an integer, $\tau_{\text{probe laser}}$ is the repetition time of the probe laser and we assume there is no jitter in $\tau_{\text{probe laser}}$. Since we run the experiment at 500 kHz, $\tau_{\text{probe laser}} = 2\ \mu$s and $N \approx 300$.

B. Time-of-flight measurement

Shown in Figure 2, the setup consists of a 40 ps full-width at half maximum (FWHM) pulsed 1550 nm laser, triggered at 500 kHz by an external function generator, that sends photons through a variable attenuator into a DWDM, which multiplexes the ToF and WR signals. Due to the short fiber length between NIST 1 and NIST 2, a variable attenuator is inserted after the first and before the second beam splitter to maintain an adequate signal strength such that the SNSPD does not saturate and that the short path has comparable attenuation as the long loopback

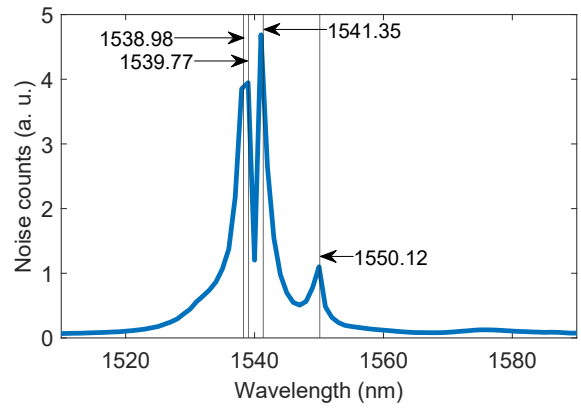

Fig. 4. The spectrum of light as measured in NIST 1 after the DWDM and the beam splitter, but before the channel 34 filter. The peaks at 1538.98 nm, 1539.77 nm, and 1541.35 nm correspond to the three WR signals, and the peak at 1550.12 nm corresponds to the ToF signal.

fiber of around 40 dB. The SNSPD had a FWHM jitter of less than 20 ps and has an impendance-matched differential design similar to that reported in [14]. One beam splitter output is directed through a short loopback from NIST 2 to NIST 1, while the other output is coupled into the DWDM and loops back from the lab at the JQI. Since the laser and detector system in NIST 1 are in a different lab from the WRS in NIST 2, the short loopback cancels the effects of drift caused by the approximately 250 m of fiber between NIST 1 and NIST 2. The signals from the short loopback and the JQI loopback are then coupled into the same fiber by the second beam splitter. This signal is then sent through a single DWDM channel-34 filter to remove the classical signal noise in the same fiber, and finally it is detected by the SNSPD and logged by the time tagger with 2 ps internal timing resolution. Finally, the time tagger accumulates a histogram of photon arrival times. We identify the two peaks in the histogram to obtain the photons' mean arrival times for the short and JQI loopbacks. We subtract two arrival times to obtain the time difference between the direct loopback and the JQI loopback, which is logged as the roundtrip time, $\Delta t'_{\mathrm{ToF}}$ (related to the actual roundtrip time by Eq. 4).

An important parameter for the experiment is the integration or averaging time, that is the length of time for which the histogram accumulates photon counts before resetting. We first chose a minimum integration time, $\tau_0 = 100$ ms. Over a period of time, typically half a day, a histogram is accumulated every 100 ms, and the peak differences corresponding to the photons' roundtrip time is calculated for the 100 ms measurement, producing data set $\overline{\Delta t'}_{\mathrm{ToF},i}(\tau_0)$. For integration time $\tau = M\tau_0$, we average every M measurements to produce the data set $\overline{\Delta t'}_{\mathrm{ToF},i}(\tau)$ (for instance, by averaging over every two 100-ms measurements for τ =200 ms). We then evaluated the standard deviation $\sigma_{\mathrm{ToF}}(\tau)$ where

$$\sigma^2_{\mathrm{ToF}}(\tau) = \frac{1}{2}\langle(\overline{\Delta t'}_{\mathrm{ToF},i+1}(\tau) - \overline{\Delta t'}_{\mathrm{ToF},i}(\tau))^2\rangle. \tag{5}$$

The expectation value is calculated over the data set indexed by parameter i. Figure 3 shows σ_{ToF} vs. averaging times for three separate loopback experiments, the WR roundtrip time estimate, and the NIST internal loopback. We note that the WR data was

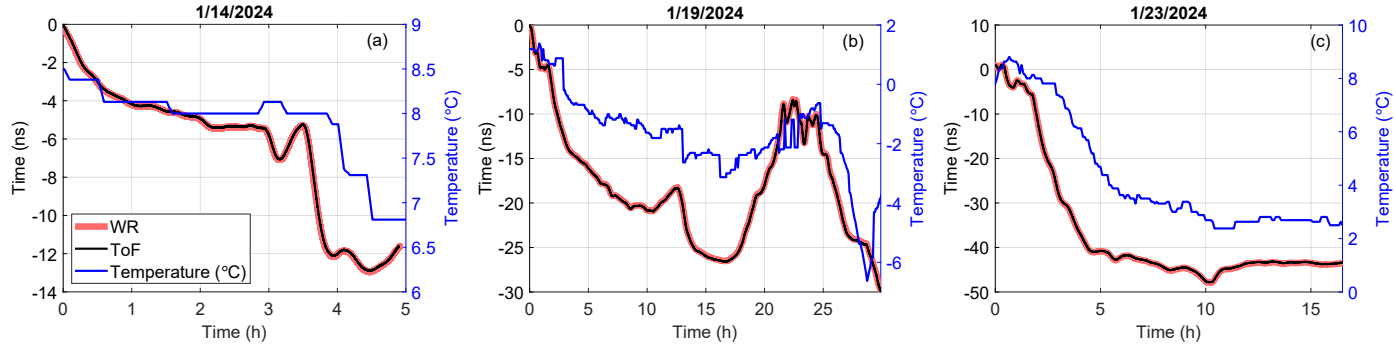

Fig. 5. Relative WR and roundtrip ToF times for (a) 1/14/2024, (b) 1/19/2024, and (c) 1/23/2024 plotted with outdoor weather data [15]. The plots are shifted such that both the ToF roundtrip time and the WR roundtrip time start at 0 ns, hence tracking only the relative roundtrip time. The plotted temperature is the aerial temperature at NIST.

taken on 1/23/2024. σ_{ToF} is similar but not exactly equal to the time deviation, TDEV [16].

Due to short-term random fluctuations (mainly caused by detector jitter and non-zero laser pulse width) σ_{ToF} at short integration times is higher, but decreases according to averaging white noise down to a minimum, after which σ_{ToF} increases. The reason for this increase is that at longer integration times, the roundtrip time will drift due to environmental effects on the fiber loopback, such as outdoor changes in temperature causing fiber length fluctuations. We note that the total roundtrip fiber loop from NIST to JQI is approximately 120 km, with 75 % of the fiber being aerial. Therefore, an optimal integration time that minimizes the uncertainty in the roundtrip estimate can be found at the minimum of σ_{ToF} plot. For these experiments we found an optimal integration time for the ToF measurement of 500 ms, which resulted in an uncertainty of approximately 2 ps (or 500 μm fiber length estimate) for the 120 km roundtrip time measurement. Also shown in Figure 3 are the σ_{ToF} values we derived from the internal NIST1-NIST2 loopback measurements. The internal measurements clearly exhibit higher stability compared to the NIST-JQI, supporting the idea that higher σ_{ToF} values for our 120 km roundtrip measurements are due to environmental changes of the long aerial fiber.

Figure 4 shows a measurement of the spectrum of light measured before the single channel-34 filter at NIST 1. Notice that despite the use of the DWDM to isolate the individual wavelengths in the returning multiplexed signal, there are still 3 peaks at 1538.98 nm, 1539.77 nm, and 1541.35 nm, which are the wavelengths of the three WR signals as shown in figure 1. These peaks are due to cross-talk in the DWDM leading the WR signals to interfere with the ToF signal, resulting in significant noise. Hence, the single DWDM channel-34 filter is necessary to isolate the ToF signal.

3. RESULTS

Figure 3 shows a plot of σ_{ToF} for the three JQI loopback data sets, along with a σ_{ToF} plot of the NIST internal loopback. For longer integration times, the σ_{ToF} plots for the JQI loopback data sets are similar, indicating that the noise sources on longer time scales are similar. However, the σ_{ToF} values differ more significantly at shorter integration times, which we speculate to be from noise on shorter time scales, such as temperature and wind environmental fluctuations.

The relative ToF roundtrip and WR roundtrip times for data collected on January 14, 2024, January 19, 2024 and January 23, 2024 are shown in figure 5. Since we are only interested in the relative WR and ToF times, we set the relative times equal to zero at the start of each measurement data set. Each plot also shows the outdoor ambient temperature at NIST during each measurement. As the temperature increases, the refractive index of the fiber and the fiber length increases, leading to a longer roundtrip time. Hence, both the ToF roundtrip and the WR roundtrip time curves qualitatively follow the temperature. Since the temperature data is only measured at one location (the aerial temperature at NIST), it does not account for varying temperature along the whole fiber length, which we expect to be varying over the ≈60 km fiber length. Also, around 25 % of the fiber is underground and is probably not subject to the changes in aerial temperature and sun exposure.

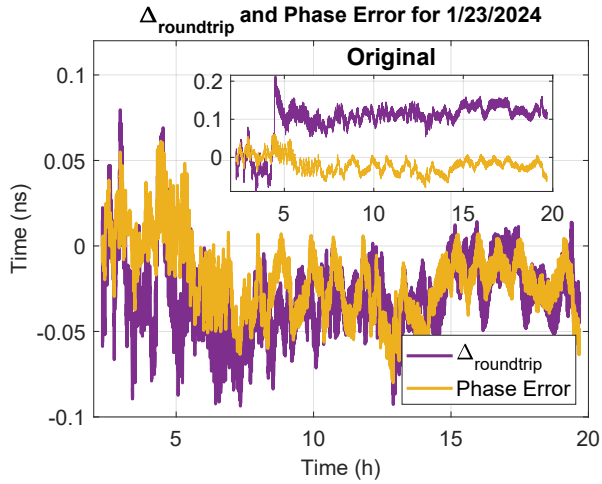

Fig. 6. Corrected version of the $\Delta_{\mathrm{roundtrip}}$ and WR phase error plot. Inset shows the original data. The correction consists of assuming a fixed, step offset in the WR error occurring at ≈4.45 hours and subtracting this offset for data at times after the occurrence of the step offset.

In order to see the difference between the ToF and the WR roundtrip times, we define $\Delta_{\mathrm{roundtrip}} = \Delta t_{\mathrm{ToF}} - \Delta t_{\mathrm{WR}}$ as the difference between the two roundtrip times. Figure 6 plots the $\Delta_{\mathrm{roundtrip}}$ and the phase error between the two WRS clocks at NIST 2, $\varepsilon_{\mathrm{clock}}$, for the entire experimental run on January 23rd, 2024. We noticed that at approximately 4.45 hours, there was a sharp increase in the roundtrip time estimated by the WR.

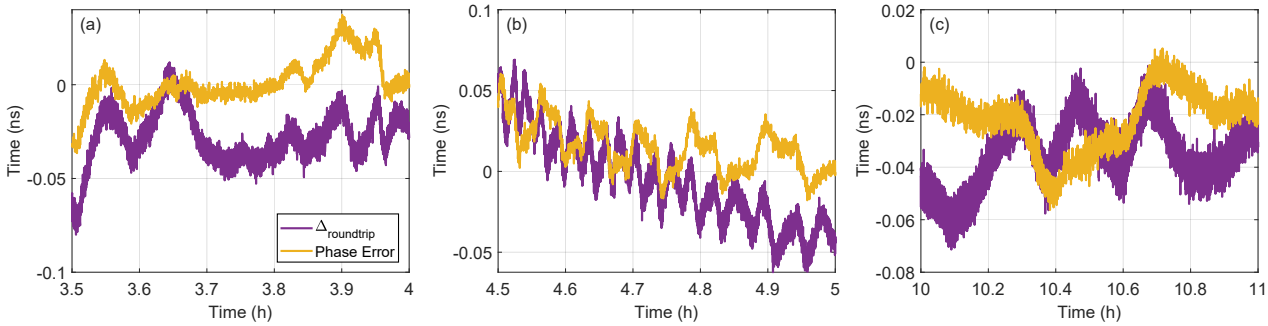

Fig. 7. Zoomed in plot of the $\Delta_{\text{roundtrip}}$ and phase error plot at three different times. Notice that the frequency of the $\Delta_{\text{roundtrip}}$ oscillations is around twice that of the phase-error oscillations.

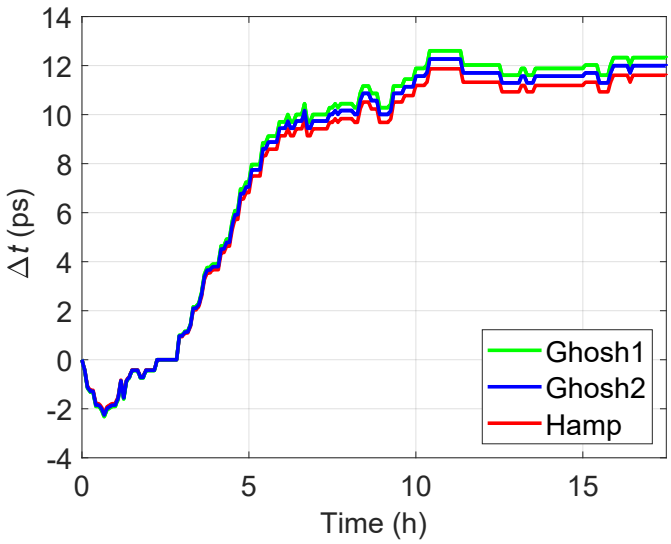

Fig. 8. Estimate of deviation $\Delta t_{\text{ToF}} - \Delta t_{\text{WR}}$ due to temperature-dependent dispersion calculated from the dispersion functions "Ghosh1", "Ghosh2" and "Hamp". The estimate is based on the temperature data over ≈17 hours of the experiment on 1/23/2024. $\Delta t_{\text{ToF}} - \Delta t_{\text{WR}}$ is taken to be zero at the start of the measurement.

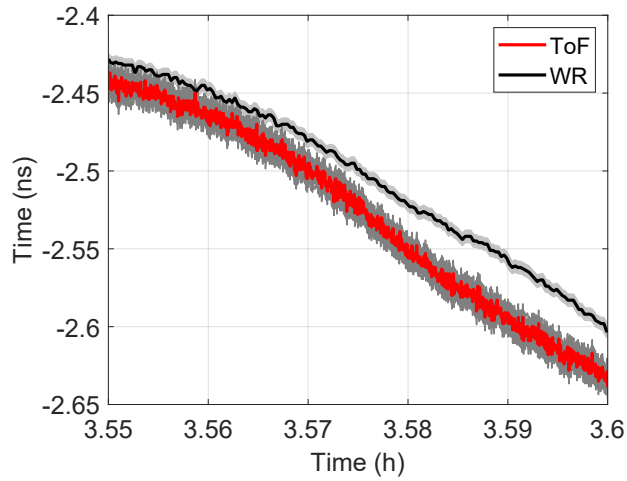

Fig. 9. Zoomed in plot of the ToF and the WR relative roundtrip times for 1/23/2024. The gray-shaded regions represent 95 % confidence intervals. We emphasize that the ToF roundtrip and WR roundtrip times are relative. At this scale, one is able to see the drift in $\Delta_{\text{roundtrip}}$ and notice that the ToF and WR roundtrip times have a statistically significant disagreement.

We speculate that this discontinuity is caused by an error in the roundtrip time reported by the WR. Assuming that the ToF roundtrip time can be regarded as the reference, we realign the WR roundtrip time at 4.45 hours such that the difference in roundtrip times, $\Delta_{\text{roundtrip}}$, is continuous across the irregularity.

Figure 7 shows a zoom-in of particular sections of data presented in figure 6. We notice oscillations in $\Delta_{\text{roundtrip}}$ and the phase error are approximately equal in amplitude. However, the oscillation frequency of $\Delta_{\text{roundtrip}}$ is approximately double that of the phase error from the WR clocks. While we cannot offer an explanation on the observed behavior, we believe that the ToF measurement can be utilized to achieve a high-precision roundtrip time measurement. Specifically, the ToF measurements can be used to update the WR asymmetry coefficient, α, to reflect real-time change in the fiber and updated one-way delay estimation, which will improve the precision compared to the round trip delay measurements derived from the statically calibrated α coefficient. More studies are needed to understand how the ToF measurement can be integrated to improve real-time path delay estimates in the WR system.

The ToF and WR roundtrip time measurements exhibit good agreement throughout the duration of the experiment, as seen in figure 5. To investigate the deviation between the ToF and WR roundtrip time measurements, let us first consider their measurement uncertainties. For Δt_{WR}, we can estimate the uncertainty, $u(\Delta t_{\text{WR}})$, from the σ_{ToF} plot (figure 3). The averaging time that produces the minimum σ_{ToF} is 1 s, at which point σ_{ToF} equals 2.0 ps. We therefore estimate the measurement uncertainty for the WR roundtrip time to be $u(\Delta t_{\text{WR}}) = 2$ ps.

For the uncertainty in Δt_{ToF}, $u(\Delta t_{\text{ToF}})$, there are contributions from σ_{ToF}, $u(\Delta t_{\text{ToF}})_{\sigma_{\text{ToF}}}$, and from the fact that the probing wavelength between the ToF and WR measurements were different, $u(\Delta t_{\text{ToF}})_{\lambda}$. For $u(\Delta t_{\text{ToF}})_{\sigma_{\text{ToF}}}$, we used the σ_{ToF} measurement to determine the optimal averaging time and associated σ_{ToF} value for the 1/23/2024 dataset; an averaging time of 0.5 s gave σ_{ToF} = 1.8 ps, so we estimate $u(\Delta t_{\text{ToF}})_{\sigma_{\text{ToF}}} = 1.8$ ps. The measurement uncertainty arising from different probe wavelengths is due to a combination of temperature-dependent chromatic dispersion in the fiber and operating temperature uncertainty. In figure 5c, we see that the temperature for 1/23/2024 ranged from about

2 °C to 9 °C. We perform an analysis of the effect of temperature on the roundtrip time measurement in the presence of chromatic dispersion in Appendix A. The results of this analysis are shown in figure 8, which shows that temperature changes between 2 °C to 9 °C result in deviations between the ToF and WR roundtrip time estimates ranging from -2 ps to 12 ps. To estimate the contribution of temperature-dependent chromatic dispersion to the uncertainty, we model the time deviation as a uniform distribution with width 14 ps. The relation between the width of a uniform distribution, w, and its standard deviation, σ, is $w = 2\sigma\sqrt{3}$. Thus we estimate the contribution to $u(\Delta t_{\mathrm{ToF}})_\lambda$ due to temperature-dependent chromatic dispersion is $u(\Delta t_{\mathrm{ToF},\lambda}) = 7/\sqrt{3} = 4.0$ ps. The two contributions combine in quadrature as

$$u(\Delta t_{\mathrm{ToF}}) = \sqrt{u(\Delta t_{\mathrm{ToF}})_{\sigma_{\mathrm{ToF}}}{}^2 + u(\Delta t_{\mathrm{ToF}})_\lambda{}^2} \tag{6}$$

to produce an estimate for $u(\Delta t_{\mathrm{ToF}}) = 4.4$ ps.

We can take into account measurement uncertainty when examining the deviations between the ToF and WR roundtrip time measurement. Figure 9 shows a zoom-in of the data taken on 1/23/2024, where the shaded regions represent the 95 % confidence interval, calculated based on the estimates for σ_{WR} and σ_{ToF} discussed above. There are regions in figure 9 where the disagreement exceeds the uncertainty estimate, which suggests there may be some other effects leading to disagreement of approximately 10 ps between the WR and ToF roundtrip time measurements.

4. CONCLUSION

In conclusion, we presented a measurement method based on single-photon ToF that is naturally suited to measure fiber-link-length changes in quantum networks. There is good agreement between the single-photon ToF and WR-PTP roundtrip time estimates of a deployed ≈120-km optical fiber link that includes both aerial and underground fiber. We found correlation between the phase error of two WR clocks and the difference of the ToF and WR fiber roundtrip time estimates, $\Delta_{\mathrm{roundtrip}}$. The single-photon ToF can be integrated as an in-situ time-of-flight measurement for OTWTFT methods, such as WR-PTP, to achieve higher precision time transfer.

5. ACKNOWLEDGMENTS

This work was supported by the Quantum Information Science Initiative (QISI) and National Quantum Initiative (NQI). Contribution of NIST, an agency of the U.S. government, not subject to copyright. The authors thank Mheni Merzouki, Bruce Crabill, Oliver Slattery and Abdella Battou for their assistance on the deployed fiber link between NIST and UMD.

6. DISCLOSURES

The authors declare no conflicts of interest. Any mention of commercial products or reference to commercial organizations is for information only; it does not imply recommendation or endorsement by NIST, nor does it imply that the products mentioned are necessarily the best available for the purpose.

A. TEMPERATURE-DEPENDENT DISPERSION

Optical fiber can exhibit temperature-dependent dispersion [17–20], causing a change in the refractive index as a function of wavelength and temperature. In our experiment, the ToF and WR signals were separated by about 10 nm, and temperature-dependent chromatic dispersion will cause differences in the roundtrip time estimate. We therefore must account both for the change in round-trip-time measurement caused by performing the measurements at different wavelengths and deviations caused by temperature. In this appendix, we estimate the deviation in round-trip-time measurements caused by the temperature-dependent chromatic dispersion.

There have been various efforts to study the temperature dependence of chromatic dispersion in optical fibers [18, 19, 21, 22]. We use standard SMF28 optical fiber, which is a single-mode step-index fiber well-described by dispersion formulas given in [22–24]. Ref. [23] gives formulas for the refractive index, $n(\lambda, T)$ as a function of wavelength, λ, and temperature, T. Ref. [22] studies optical fibers and presents expressions for the dispersion parameter, D, and its temperature dependence. The parameter, D, is related to the refractive index, n and group index, n_g by

$$D = \frac{1}{c}\frac{dn_g}{d\lambda} = -\frac{\lambda}{c}\frac{d^2n}{d\lambda^2}, \tag{7}$$

where c is the speed of light. Ref. [24] presents dn/dT for fiber glasses, which can be combined and used to calculate the temperature dependence of n.

In Ghosh's work [23], the refractive index, $n(\lambda)$, (or Sellmeier equation) is written as:

$$n^2 = A + \frac{B}{1 - C/\lambda^2} + \frac{D}{1 - E/\lambda^2}, \tag{8}$$

where λ is the wavelength given in microns. Temperature dependence is incorporated by parameters of the form $X = mT + c_1$, where X is a Sellmeier coefficient (that is A, B, C or D in Eq. 8), T is the temperature in degrees Celsius, and m and c_1 are empirically determined coefficients, which we list here for clarity

$$\begin{aligned} A &= 6.90754 \times 10^{-6}T + 1.31552 \\ B &= 2.35835 \times 10^{-5}T + 0.788404 \\ C &= 5.844758 \times 10^{-7}T + 1.10199 \times 10^{-2} \\ D &= 5.48368 \times 10^{-7}T + 0.91316 \\ E &= 100. \end{aligned} \tag{9}$$

We will refer to this model as "Ghosh1."

In a separate paper, Ghosh [24] presents the following dependence of the refractive index on temperature:

$$2n\frac{dn}{dT} = GR + HR^2, \tag{10}$$

where $R = \lambda^2/(\lambda^2 - \lambda_g^2)$ is the normalized wavelength, λ is the wavelength in microns, and G, H and λ_g are fitted temperature parameters of the material. From [24], we use the values $\lambda_g = 0.109\ \mu$m, $G = -1.6548 \times 10^{-6}$ °C^{-1}, and $H = 3.17794 \times 10^{-5}$ °C^{-1}.For n in Eq. 10, we use n from Table I in Ref. [23] with parameters for Eq. 8 as

$$\begin{aligned} A &= 1.3121622 \\ B &= 0.79525205 \\ C &= 1.10996732 \times 10^{-2} \\ D &= 0.9116877 \\ E &= 116. \end{aligned} \tag{11}$$

We chose $E = 116$ to set the zero-dispersion wavelength to 1313 nm to match that for SMF28. We use this same n for $n(T_0)$ to

calculate $n(\lambda, T) = n(T_0) + (T - T_0)dn/dT$, where $T_0 = 26\ ^\circ$C. We will refer to this model as "Ghosh2."

Finally, in Hamp's work [22], temperature dependence is taken into account by a relation of the form:

$$\frac{dD}{dT} = \frac{1}{4}\left(\lambda - \frac{\lambda_0^4}{\lambda^3}\right)\frac{dS_0}{dT} - \frac{S_0\lambda_o^3}{\lambda^3}\frac{d\lambda_0}{dT}, \tag{12}$$

where λ_0 is the zero dispersion wavelength, S_0 is the dispersion slope at λ_0, and D is the dispersion parameter, which is related to the refractive index, n by Eq. 7. We use parameters from Ref. [22] for a non-dispersion shifted fiber having λ_0 close to the zero-dispersion wavelength for SMF28

$$\begin{aligned} \lambda_0 &= 1320.61 \text{ nm} \\ S_0 &= 9.143 \times 10^{-2} \text{ ps/nm/nm/km} \\ d\lambda_0/dT &= 0.026 \text{ nm}/^\circ\text{C} \\ dS_0/dT &= -0.4 \times 10^{-6} \text{ ps/nm/nm/km}/^\circ\text{C}. \end{aligned} \tag{13}$$

We will refer to this model as "Hamp."

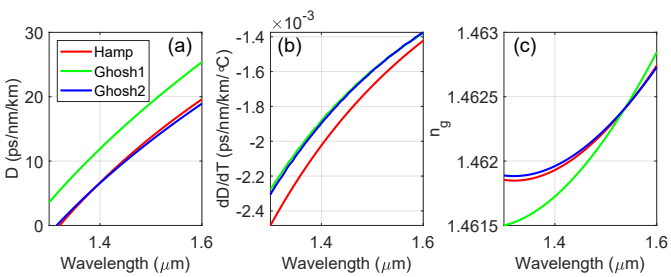

Fig. 10. Comparison of the (a) dispersion parameter, D, (b) temperature dependence of the dispersion, dD/dT, and (c) group index, calculated using the methods "Hamp", "Ghosh1", and "Ghosh2". There is good agreement in the calculated results using the three dispersion models.The temperature for these plots is 25 °C.

We compared the three models to check for consistency. Using Eq. 7, we convert Ghosh's values for $n(\lambda, T)$ to D and $\frac{dD}{dT}$. The result is shown in figure 10. Both D and $\frac{dD}{dT}$ show good agreement. The group index is needed to calculate the time-of-flight in a length of optical fiber. From Eq. 7, we see that D is proportional the derivative of the group index with respect to wavelength. We can integrate cD from "Hamp" to get n_g up to an additive constant. We fix this constant by setting $n_{g,\text{Hamp}} = n_{g,\text{Ghosh2}}$ at 1550 nm. There is good agreement in the group indices calculated by the three models (Fig. 10c).

For light pulses traveling in optical fiber, the roundtrip time is calculated using the group index $n_g = n(\lambda) - \lambda\partial n/\partial\lambda$ (see Fig. 10c). Let Δt_{ToF} be the ToF roundtrip time, and let Δt_{WR} be the WR roundtrip time at temperature, T. If we assume the fiber is at the same temperature along its full length, we can calculate the length of the fiber, $L_{\text{fiber}} = c\Delta t_{\text{ToF}}/n_{g,\text{ToF}} = c\Delta t_{\text{WR}}/n_{g,\text{WR}}$, where $n_{g,\text{ToF}}$ and $n_{g,\text{WR}}$ are the group refractive indices at temperature, T, at the ToF wavelength (1550.12 nm) and WR wavelength (1539 nm), respectively. Rearranging this expression, we find the ToF and WR roundtrip times are related by $\Delta t_{\text{ToF}} = \Delta t_{\text{WR}} n_{g,\text{ToF}}/n_{g,\text{WR}}$ and the difference $\Delta t_{\text{ToF}} - \Delta t_{\text{WR}} = \Delta t_{\text{WR}}(n_{g,\text{ToF}}/n_{g,\text{WR}} - 1)$. In figure 8, we use $n_g(\lambda, T)$ to calculate $\Delta t_{\text{ToF}} - \Delta t_{\text{WR}}$ based on the aerial temperature reported at NIST (the blue curve in Fig. 5c). We assume $\Delta t_{\text{ToF}} - \Delta t_{\text{WR}} = 0$ at the start of the measurement (time = 0). To apply the "Hamp" model to estimate $\Delta t_{\text{ToF}} - \Delta t_{\text{WR}}$, we utilize dD/dT as

$$\Delta t_{\text{ToF}} - \Delta t_{\text{WR}} \approx \frac{dD}{dT}(\lambda_{\text{ToF}} - \lambda_{\text{WR}})(T - T_{\text{ref}})L_{\text{fiber}}, \tag{14}$$

where T_{ref} is the temperature at the start of the measurements (where $\Delta t_{\text{ToF}} - \Delta t_{\text{WR}} = 0$), and L_{fiber} is estimated from a measurement of the roundtrip time. Specifically, at the start of the measurement Δt_{WR} was found to be 609.69 μs, and the group index for that wavelength and temperature was 1.46229, leading to an estimate of the fiber length of $L_{\text{fiber}} = 125.00$ km. We used $\lambda_{\text{ToF}} - \lambda_{\text{WR}} = 11.12$ nm, the reported aerial temperature at NIST, and Eq. 14 to estimate the difference in roundtrip time $\Delta t_{\text{ToF}} - \Delta t_{\text{WR}}$ due to temperature-dependence dispersion. Results of these calculations are plotted in Figure 8.

REFERENCES

1. J. M. Thomas, G. S. Kanter, and P. Kumar, "Designing noise-robust quantum networks coexisting in the classical fiber infrastructure," Opt. Express **31**, 43035–43047 (2023).
2. A. Rahmouni, P. S. Kuo, Y. S. Li-Baboud, I. A. Burenkov, Y. Shi, M. V. Jabir, N. Lal, D. Reddy, M. Merzouki, L. Ma, A. Battou, S. V. Polyakov, O. Slattery, and T. Gerrits, "100-km entanglement distribution with coexisting quantum and classical signals in a single fiber," J. Opt. Commun. Netw. **16**, 781–787 (2024).
3. M. Lipiński, T. Włostowski, J. Serrano, and P. Alvarez, "White rabbit: a PTP application for robust sub-nanosecond synchronization," in *2011 IEEE International Symposium on Precision Clock Synchronization for Measurement, Control and Communication,* (2011), pp. 25–30.
4. T. Gerrits, I. A. Burenkov, Y. Li-Baboud, A. Rahmouni, D. M. Anand, Hala, O. Slattery, A. Battou, and S. V. Polyakov, "White rabbit-assisted quantum network node synchronization with quantum channel coexistence," in *Conference on Lasers and Electro-Optics,* (Optica Publishing Group, 2022), p. FM1C.2.
5. W. McKenzie, Y. S. Li-Baboud, M. Morris, G. Baumgartner, A. Rahmouni, P. Kuo, O. Slattery, B. Crabill, M. Merzouki, A. Battou, and T. Gerrits, "Sub-200 ps quantum network node synchronization over a 128 km link white rabbit architecture," in *2023 Conference on Lasers and Electro-Optics (CLEO),* (2023), pp. 1–2.
6. "IEEE standard for a precision clock synchronization protocol for networked measurement and control systems," IEEE Std 1588-2019 (Revision ofIEEE Std 1588-2008) pp. 1–499 (2020).
7. "ISO/IEC/IEEE international standard - telecommunications and exchange between information technology systems–requirements for local and metropolitan area networks–part 3: Standard for ethernet," ISO/IEC/IEEE 8802-3:2021(E) pp. 1–5196 (2021).
8. ITU-T G.8262, *Timing Equipment of Synchronous Ethernet.*
9. P. Moreira and I. Darwazeh, "Digital femtosecond time difference circuit for CERN's timing system," in *Proc. London Commun. Symp,* (2011), pp. 1–4.
10. J. Serrano, M. Lipinski, T. Wlostowski, E. Gousiou, E. van der Bij, M. Cattin, and G. Daniluk, "The White Rabbit Project," in *IBIC 2013,* (Oxford, UK, 2013).
11. D. W. Allan and H. Daams, "Picosecond time difference measurement system," in *29th Annual Symposium on Frequency Control,* (1975), pp. 404–411.
12. P. Křen, "Improved digital dual-mixer time-difference technique and its applications," Measurement **192**, 110929 (2022).
13. G. Daniluk, "White rabbit calibration procedure v1.1," (2015). https://white-rabbit.web.cern.ch/documents/WR_Calibration-v1.1-20151109.pdf.
14. M. Colangelo, B. Korzh, J. P. Allmaras, A. D. Beyer, A. S. Mueller, R. M. Briggs, B. Bumble, M. Runyan, M. J. Stevens, A. N. McCaughan, D. Zhu, S. Smith, W. Becker, L. Narváez, J. C. Bienfang, S. Frasca, A. E. Velasco, E. E. Ramirez, A. B. Walter, E. Schmidt, E. E. Wollman,

M. Spiropulu, R. Mirin, S. W. Nam, K. K. Berggren, and M. D. Shaw, "Impedance-matched differential superconducting nanowire detectors," Phys. Rev. Appl. **19**, 044093 (2023).

15. Tomorrow.io, "Tomorrow docs v.4.0.1 weather data layers," (2024). https://docs.tomorrow.io/reference/weather-data-layers, Last accessed on 2024-10-11.
16. W. Riley and D. Howe, "Handbook of frequency stability analysis," (2008).
17. G. Stepniewski, R. Kasztelanic, D. Pysz, R. Stepien, M. Klimczak, and R. Buczynski, "Temperature sensitivity of chromatic dispersion in nonlinear silica and heavy metal oxide glass photonic crystal fibers," Opt. Mater. Express **6**, 2689–2703 (2016).
18. T. Kato, Y. Koyano, and M. Nishimura, "Temperature dependence of chromatic dispersion in various types of optical fiber," Opt. Lett. **25**, 1156–1158 (2000).
19. P. Andre, A. Pinto, and J. Pinto, "Effect of temperature on the single mode fibers chromatic dispersion," in *Proceedings of the 2003 SBMO/IEEE MTT-S International Microwave and Optoelectronics Conference - IMOC 2003. (Cat. No.03TH8678),* vol. 1 (2003), pp. 231–234 vol.1.
20. A. Rahmouni, N. Azami, and F. Abdi, "Numerical analysis of athermal DPSK based on unbalanced thermally expanded core optical fibers Mach Zehnder interferometer," 2010 5th Int. Symp. on I/V Commun. Mob. Networks, ISIVC 2010 (2010).
21. G. Ghosh, "Sellmeier coefficients and dispersion of thermo-optic coefficients for some optical glasses," Appl. Opt. **36**, 1540–1546 (1997).
22. M. Hamp, J. Wright, M. Hubbard, and B. Brimacombe, "Investigation into the temperature dependence of chromatic dispersion in optical fiber," IEEE Photonics Technol. Lett. **14**, 1524–1526 (2002).
23. G. Ghosh, M. Endo, and T. Iwasaki, "Temperature-dependent Sellmeier coefficients and chromatic dispersions for some optical fiber glasses," J. Light. Technol. **12**, 1338–1342 (1994).
24. G. Ghosh, "Temperature dispersion of refractive indexes in some silicate fiber glasses," Photonics Technol. Lett. IEEE **6**, 431 – 433 (1994).